Simulations of chemical vapor deposition diamond film growth using a kinetic Monte Carlo model and two-dimensional models of microwave plasma and hot filament chemical vapor deposition reactors

P. W. May,[1,a)] J. N. Harvey,[1] N. L. Allan,[1] J. C. Richley,[1] and Yu. A. Mankelevich[2]
[1]*School of Chemistry, University of Bristol, Bristol BS8 1TS, United Kingdom*
[2]*Skobel'tsyn Institute of Nuclear Physics, Moscow State University, Leninskie gory, Moscow 119991, Russia*

(Received 23 September 2010; accepted 15 October 2010; published online 9 December 2010)

A one-dimensional kinetic Monte Carlo (KMC) model has been developed to simulate the chemical vapor deposition of a diamond (100) surface under conditions used to grow single-crystal diamond (SCD), microcrystalline diamond (MCD), nanocrystalline diamond (NCD), and ultrananocrystalline diamond (UNCD) films. The model considers adsorption, etching/desorption, lattice incorporation and surface migration but not defect formation or renucleation processes. Two methods have been devised for estimation of the gas phase concentrations of species at the growing diamond surface, and are used to determine adsorption rates for C_1H_x hydrocarbons for the different conditions. The rate of migration of adsorbed carbon species is governed by the availability of neighboring radical sites, which, in turn, depend upon the rates of H abstraction and of surface-radical migration. The KMC model predicts growth rates and surface roughness for each of diamond types consistent with experiment. In the absence of defect formation and renucleation the average surface diffusion length, ℓ, is a key parameter controlling surface morphology. When $\ell<2$, surface migration is limited by the lack of availability of surface radical sites, and the migrating surface species simply hop back and forth between two adjacent sites but do not travel far beyond their initial adsorption site. Thus, Eley–Rideal processes dominate the growth, leading to the rough surfaces seen in NCD and UNCD. The maximum or "intrinsic" surface roughness occurs for nominally zero-migration conditions ($\ell=0$) with an rms value of approximately five carbon atoms. Conversely, when migration occurs over greater distances ($\ell>2$), Langmuir–Hinshelwood processes dominate the growth producing the smoother surfaces of MCD and SCD. By extrapolation, we predict that atomically smooth surfaces over large areas should occur once migrating species can travel approximately five sites ($\ell\sim5$). β-scission processes are found to be unimportant for MCD and SCD growth conditions, but can remove up to 5% of the adsorbing carbon for NCD and UNCD growth. C_1H_x insertion reactions also contribute $<1\%$ to the growth for nearly all conditions, while C_2H_x ($x<2$) insertion reactions are negligible due their very low concentrations at the surface. Finally, the predictions for growth rate and morphology for UNCD deposition in a microwave system were found to be anomalous compared to those for all the other growth conditions, suggesting that carbonaceous particulates created in these plasmas may significantly affect the gas chemistry. © *2010 American Institute of Physics*. [doi:10.1063/1.3516498]

I. INTRODUCTION

Chemical vapor deposition (CVD) of diamond is a maturing technology that is beginning to find many commercial applications in electronics, cutting tools, medical coatings and optics.[1] The CVD process usually involves the gas-phase activation of a gas mixture containing a small quantity of a hydrocarbon in excess hydrogen.[2,3] A typical gas mixture uses a few percent CH_4 in H_2 (plus sometimes additional Ar or N_2), and depending upon the growth conditions, substrate properties and growth time, this produces polycrystalline films with grain sizes from ~5 nm to mm. Films with grain sizes less than 10–20 nm are often called ultrananocrystalline diamond (UNCD) films; those with grain sizes a few tens or hundreds of nanometers are nanocrystalline diamond (NCD); those with grain sizes microns or tens of microns are termed microcrystalline diamond (MCD); and those with grain sizes approaching or exceeding 1 mm are single crystal diamond (SCD).

However, to obtain a diamond film with the desired morphology combined with controlled electronic and mechanical properties requires a detailed understanding of the many parameters affecting growth, such as the substrate temperature, gas mixture, process pressure, etc. The so-called 'standard growth mechanism'[4] developed in the early 1990s is a reasonably robust description of the general CVD diamond process, although it fails to fully explain many of the complexities of growth, such as the growth rate and crystal size of polycrystalline films. In this model, atomic H created by thermal or electron-impact dissociation of H_2 is the driving force behind all the chemistry. It is widely accepted[5,6] that the main growth species in standard diamond CVD is the CH_3 radical, which adds to radical sites ("dangling bonds") created on the diamond surface following hydrogen abstrac-

a)Electronic mail: paul.may@bris.ac.uk.

 © 2010 American Institute of Physics

Downloaded 10 Dec 2010 to 137.222.40.127. Redistribution subject to AIP license or copyright; see http://jap.aip.org/about/rights_and_permissions

tion by H atoms. The fraction of surface carbon atoms, F, which support such radical sites is the result of dynamic equilibrium between H abstraction and H addition reactions which are dependent upon the process conditions, especially the concentration of gas phase atomic H just above the surface, $[H]_s$, and the substrate temperature, T_s. Under typical CVD diamond conditions $F \sim 0.1$, i.e., $\sim 10\%$ of the surface supports radical sites.

An elevated substrate temperature (typically $T_s > 700$ °C) allows migration of the adsorbed carbon species across the surface until they meet a step-edge and add to the diamond lattice (so-called "step-flow growth"),[7] or are removed back to the gas phase by an etching process. Another proposed role for the atomic H is to preferentially etch into the gas phase any adsorbed carbon groups that have deposited as non-diamond phases, while for the most part sp^3 carbon species are left behind. However, the etch rate of surface sp^3 hydrocarbon species is not zero and depends upon their location. As such, it provides an alternative explanation for growth via step-edges. Such 'preferential etching'[8] means that sp^3 hydrocarbon species adsorbed on flat diamond surfaces are etched away faster than those adsorbed next to a step-edge, resulting in hydrocarbon species preferentially residing at step-edges. It is believed that hydrocarbons C_xH_y with two or more carbons ($x \geq 2$) are prevented from contributing to the growth by the "β-scission" reaction[4] which is a rapid, low energy, efficient process that stops the build-up of long-chained molecules on the growing surface. Therefore, in this standard model, diamond growth is seen as a competition between etching and deposition, with carbons being added to and removed from the diamond surface on an atom-by-atom basis.

Surface migration of carbon species is still a somewhat contentious issue, and the mechanism and role it plays in growth remains unclear. Chemisorbed molecular groups, such as CH_2, can, in principle, migrate along or across a dimer row so long as they have an adjacent radical site into which to move. Because these radical sites are created by H abstraction reactions, the migration process can be considered to be mediated by the local atomic H concentration since this determines abstraction rate. Such chemical migration has been modeled in the group of Frenklach,[9–11] and their estimated migration length of ~ 10 Å is consistent with the experimentally observed terrace sizes.[12] Detailed calculations of potential energy surfaces for migration steps on the (100) and (111) surfaces have also been performed using more accurate methods by Cheesman *et al.*[13] and Larsson *et al.*,[14] respectively, and both groups confirm the existence of low overall barriers for migration, suggesting very rapid intrinsic "hopping" rates at higher T_s values.

Our group recently developed a modified version of the standard growth model which considers the effects of all the C_1 hydrocarbon radicals (CH_3, CH_2, CH, and C atoms) on both monoradical and biradical sites on a (100) diamond surface.[15] Our growth model also relies upon surface migration of CH_2 groups along and across the reconstructed dimer rows in order to predict growth rates to within a factor of two of experimental observations, but it has an advantage in also being able to predict the average grain size in the resulting polycrystalline film, which can vary from a few nanometers in UNCD films to millimeters for MCD films.

Despite the successes of both growth models, direct evidence for surface migration, nucleation processes, the effects of gas impurities and gas-surface reactions remain sparse and mostly circumstantial. Due to the difficulties of obtaining direct evidence for many of the gas-surface processes by experimental means, various workers have turned to theoretical models of these interactions, such as kinetic Monte Carlo (KMC) simulations. In KMC, a model of the diamond surface is created and a set of relevant processes and mechanisms are constructed, including those in which C species (usually CH_3) are allowed to strike the surface randomly with an overall average impact rate. Some of these will adsorb with probability given by the rates estimated from experiment or theoretical models. Another possibility in the KMC simulations is to allow migration of the adsorbed C species to an adjacent site, the probability of which depends on the magnitude of the activation barrier, the surface temperature, and the pre-exponential (attempt) frequency. When the C species meets the bottom of a step-edge, the species may bond to the edge thereby extending the diamond structure, with a probability related to the results of detailed calculations previously carried out based on geometries, steric effects and energies, and kinetic data. Given sufficient numbers of impinging methyls and sufficient computing time, the growth of many layers of diamond can be simulated.

One of the most successful recent KMC implementations is that of Netto and Frenklach,[16] which used methyl radicals as the only growth species, with incorporation of C into the diamond structure described by a ring-opening/closing mechanism. CH_2 migrations along and across the dimer reconstructions were included, as well as etching of isolated CH_2 groups. The energetics and kinetic data for these reactions were obtained from numerous semiempirical electronic structure calculations and from experimental measurements. Nevertheless, some of the required rate constants remain only estimates, with varying degrees of accuracy.

With the aim of using the KMC approach to obtain insights into the overall growth mechanisms—but in reasonable timescales in terms of computing time—we developed a simplified one-dimensional KMC model of the growth of diamond films,[17] initially for a fixed set of process conditions and substrate temperature. Although the model was only one-dimensional (1D), the interplay between adsorption, etching/desorption, and addition to the lattice was qualitatively modeled using known or estimated values for the rates of each process. Color-coding the various surface species allowed the interplay between these various processes to be readily observed as the simulation progressed. We included in the model migration of sp^3-bonded CH_2 groups across the (100) diamond surface using a simplified version of the ring-opening mechanism described by Cheesman *et al.*[13]

In a follow-up paper[18] we added the possibility of surface defects to the model, and more recently we extended the KMC model of SCD growth to include the temperature dependence of the various surface processes.[19] To do so, we re-examined the values of all the kinetic parameters previously obtained from literature sources to determine their ac-

Downloaded 10 Dec 2010 to 137.222.40.127. Redistribution subject to AIP license or copyright; see http://jap.aip.org/about/rights_and_permissions

curacy and consistency with the microscopic rates for elementary processes at the diamond surface. Preliminary analysis of the etching mechanism suggested that removal of adsorbed sp^3-bonded carbon species from the diamond surface by etching or desorption was highly unlikely on thermodynamic grounds.[13] The only mechanism considered able to remove such species was β-scission, but this only accounted for removal of at most 2% of the adsorbing species. Thus, with no rapid removal process, the net growth rate was determined simply by the adsorption rate of carbon species onto the surface. Further modifications arose from separate detailed *ab initio* calculations[20] which showed that migration down a step-edge had a similar energy barrier to migration on the flat, and thus migration down steps (the "lemmings" scenario[19]) is facile. Most importantly, we modified the model for surface migration, taking better account of the fact that the migration mechanism[10,13] requires the presence of a radical site both on the initial and final positions of the migrating carbon. Under many conditions the rate-limiting step in surface migration is the rate of creation of surface radical sites, which is determined by the rate of H-abstraction reactions. Incorporating these improvements into the KMC model for typical MCD growth conditions revealed that surface migration still occurs rapidly, but is mostly limited to the adsorbed CH_2 species oscillating back and forth between two adjacent radical sites. Despite the average number of migration hops being in the thousands, the average surface diffusion length, ℓ, for a surface species—before it either adds to the diamond lattice or is removed back to the gas phase—is <2 sites. At low substrate temperature we found that migration is negligible, with film growth being dominated by direct adsorption (Eley–Rideal) processes. The resulting films were rough and spiky, reminiscent of amorphous carbon. With increasing substrate temperature, migration increases in significance until, for temperatures >1000 K, migration is the major process by which the surface becomes smoother. Under these conditions, Langmuir–Hinshelwood processes dominate (70%) the growth mechanism.

These simulations all assumed diamond growth was occurring under typical MCD growth conditions, e.g., a hot filament (HF) reactor containing a gas mixture of $1\%CH_4/H_2$ at 20 Torr, with a 2000 K filament positioned 5 mm away from a single-crystal (100) diamond substrate, but with varying substrate temperature, T_s. The concentrations of gas-phase species striking the diamond surface had been previously estimated[15] using a three-dimensional model for the activated C/H/(Ar) gas mixture which includes 200 direct and reverse reactions for 27 neutral species, electronically excited levels of H, and H_2, electrons and five ions. The model also includes the important gas-surface reactions, plus diffusion, convection and transport processes within the reactor, and its predictions have compared favorably with laser spectroscopy and *in situ* mass spectrometric measurements made in the center of the plasma or close to the filament. For a given set of process conditions this model can be used as the basis to determine the concentrations of all the major gas phase species at any position within a given reactor.

In this paper we now report the results of our KMC model using the gas chemistry and conditions employed for the growth of SCD, MCD, NCD, and UNCD. The gas chemistry activation, the species concentrations and gas temperature distributions are calculated using the previously reported models of hot-filament[21] and microwave-plasma CVD reactors mentioned above.[22] The aim is to gain insight into the roles played by the various precursor gas species in the growth process, and to ascertain their relative importance in controlling the growth rate and morphology of the resulting film.

II. MODIFICATION TO THE KMC MODEL

A full description of the KMC model for MCD conditions at different substrate temperatures has been presented in detail previously.[19] However, to simulate a more extensive range of conditions than just those used for deposition of MCD, this model required a few important modifications, which are outlined in the sections below.

A. Estimation of species concentrations at the surface

The first consideration is that for some conditions (e.g., those used for UNCD deposition) the concentrations of other C_1 species, in particular C atoms, may no longer be negligible in comparison to that of CH_3. Thus, we now need to determine the rates of adsorption for *all* relevant hydrocarbon radical species onto the surface, and decide their subsequent fates. The first task was to re-evaluate the data from the simulations of the gas-phase chemistry published previously[15] to estimate the concentrations for all the important C_1 species at the diamond surface. Figures 1(a) and 1(b) show an example of such data for SCD conditions for a sub-set of the species present. Similar data exist for MCD, NCD, and UNCD conditions (see Ref. 23). The model calculates the concentrations of species as a function of position, z, above the diamond surface, but is restricted in resolution to the grid size, the value of which was chosen to be 0.5 mm based upon the limitations of computation speed. Therefore, the data in Fig. 1 taken from Ref. 15 for species concentrations *near* the substrate equate to a distance of $z=0.5$ mm in the model. Previously we have assumed that the species concentrations at the surface ($z=0$) can be taken to be the same as those calculated at $z=0.5$ mm. However, near the surface there is often a thin boundary layer (<1 mm) in which temperatures, gas flows, and concentrations can change significantly. For previous KMC calculations, the only species that needed to be considered were H and CH_3, which [as can be seen in Fig. 1(b)] have relatively weak dependences of concentration with z for $z<5$ mm, despite the steep temperature drop over this distance. As a result, our previous assumption that the concentration of CH_3 at $z=0$ can be taken to be the same as that at $z=0.5$ mm is reasonable. However, such an assumption would be incorrect for the other hydrocarbon species, whose dependences of concentration with z near the surface are much stronger. We have tackled this problem using two approaches:

Method A: In the first approach, we found that power-law expressions of the form $[X]=pz^q$, where [X] is the con-

Downloaded 10 Dec 2010 to 137.222.40.127. Redistribution subject to AIP license or copyright; see http://jap.aip.org/about/rights_and_permissions

centration of a given species at position z, and p and q are constant fitting parameters, fitted the concentration dependences of all the species between $z=5$ to 0.5 mm reasonably accurately [see Fig. 1(b)]. Extrapolation of these expressions to smaller z allows [X] for each species to be estimated at positions closer to the surface. However, extrapolation back to $z=0$ is clearly not acceptable, as this would always give $[X]_s=0$, and also would be incorrect on physical grounds as the position and effect of any boundary layer are unknown. Therefore, a degree of subjective judgment is required as to the z-position at which the extrapolation becomes invalid. For most species this will be a moot point, as once $[X]_s$ falls below $\sim 10^9$ cm^{-3} that species will have negligible influence on the growth chemistry. Nevertheless, a position needs to be chosen, and we have used 0.05 mm as the threshold, as this is roughly equivalent to the mean free path of molecules at process pressures 100–200 Torr. In other words, we take $[X]_s \sim [X](z=0.05$ mm), and assume that the cases where this may be inaccurate (maybe even by a couple of orders of magnitude) are irrelevant since at that position [X] $< 10^9$ cm^{-3}. The extrapolated concentrations for many of the important species for five diamond deposition conditions are given in Table I.

Method B: The second approach to estimating $[X]_s$ from the data in Fig. 1 is to treat the gas close to the surface as being simply a compressed version of the gas at the top of the plasma ball (or above the filament). In doing so, we ignore the effect of any temperature jump ΔT near the substrate surface, because, for all conditions under study, calculations based on the literature data[24] for similar systems show that $\Delta T < 60$ K and is therefore negligible. With this approximation we can take the chemistry occurring at the top of the plasma ball to be an analog for that near the surface. The disadvantage of this approach is that it neglects any differences in diffusional transfer terms. The advantage is that an arbitrary extrapolation threshold is no longer needed; we simply find the z-position in the plasma at which the gas temperature is the same as the surface temperature ($T_g(z) = T_s$) and take the concentrations of all the species at this z-position, [X](z), to be an estimate for those at the surface. These values are also shown in Table I, and in most cases are similar to those obtained using the first approach.

Using either methods A or B we find that the concentration of CH_3 at the surface only decreases by a factor of 2 or 3 from that at $z=0.5$ mm, which means that previously published results[17–19] which used the higher value for $[CH_3]$ are not significantly affected and are still valid. However, the new estimated surface concentrations for many of the more reactive species, including C, CH, and CH_2, are smaller by a few orders of magnitude than their values at $z=0.5$ mm. This may have important implications for workers studying the effect of these species upon defect formation or sp^2 C content in diamond films (e.g., Refs. 25 and 26), because these new, much lower concentrations mean these species contribute far less to the growth process than previously thought. In the results that follow, we shall use method B for all data presented, noting that use of method A produces nearly identical trends. Where significant differences do occur, both sets of data are presented.

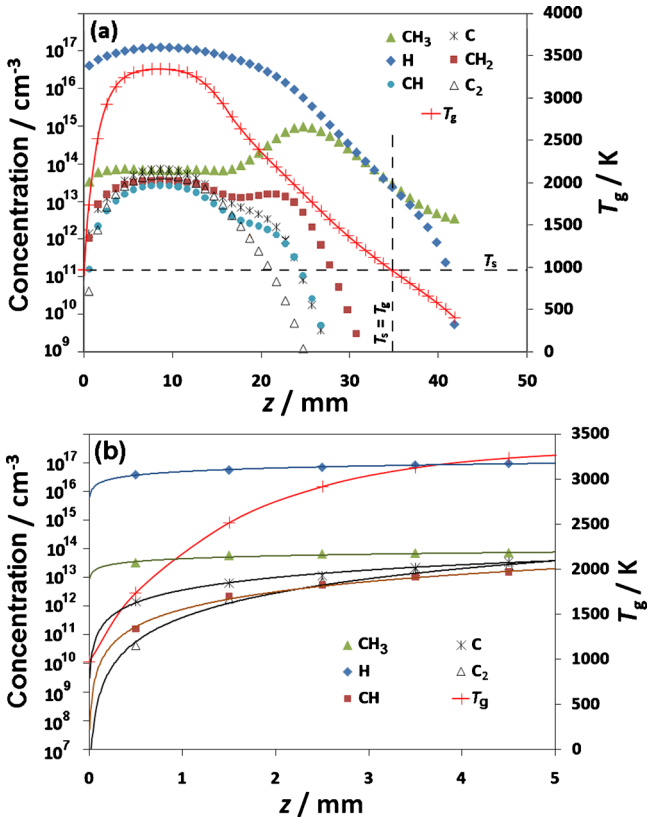

FIG. 1. (Color online) Concentrations of a sub-set of the gas-phase species above a diamond surface for MW plasma SCD conditions calculated using the model in Ref. 15. (a) The full data set from $z=0$ to 50 mm, with a dashed vertical line showing the position ($z=34.5$ mm) where the gas temperature equals the substrate temperature ($T_g=T_s$) used in method B. (b) The same data on an expanded scale near the substrate. The best-fit lines using power-law expressions used in method A are also shown with their extrapolations back to near $z=0$.

Note that the hydrogen concentration at $z=0$, $[H]_s$, is a special case as a result of the substantial loss of H atoms at the substrate and substrate-holder surfaces due to H-abstraction and addition reactions. Thus, $[H]_s$ was calculated using a more elaborate diffusion model taking account of losses and reactions at the surface (described in Ref. 15), and is also given in Table I.

B. Calculation of adsorption rates

We again assume that only C_1 species contribute to the deposition mechanism and that larger hydrocarbon radicals are simply spectators.[17] This is supported by the data in Table I which show that the new estimates (using both methods A and B) for the concentrations at the surface of C_2(a) and C_2(X) are negligible ($<10^6$ cm^{-3}) for all diamond growth conditions. Following the procedure in Ref. 15, the rate at which a given CH_x ($x=0-3$) species is adsorbed per surface radical site is given by:

$$CH_x \text{ adsorption rate} = P\bar{c}[CH_x]_s/4N_s, \quad (1)$$

where N_s is the number of C atoms per unit area of the diamond (100) surface ($\sim 1.56\times 10^{19}$ m^{-2}), and $\bar{c}$ is the mean speed of the species given by

Downloaded 10 Dec 2010 to 137.222.40.127. Redistribution subject to AIP license or copyright; see http://jap.aip.org/about/rights_and_permissions

TABLE I. Concentrations, [X], (in cm^{-3}) of selected gas-phase species near and at the surface, for different experimental diamond film growth conditions (Ref. 15).Briefly, MCD conditions are $1\%CH_4/H_2$ at 20 Torr in a HFCVD reactor with $T_s \sim 1173$ K; NCD conditions are the same except using $5\%CH_4/H_2$; UNCD(HF) conditions used the same reactor but with $80\%Ar/18.5\%H_2/1.5\%CH_4$ at 100 Torr; UNCD(MW) films were deposited using $1\%CH_4/1\%H_2/98\%Ar$ in a 700 W MW plasma at 170 W and a reduced $T_s \sim 873$ K; and SCD conditions are for a high density, 600 W MW plasma at 180 Torr using $10\%CH_4/H_2$ and $T_s \sim 973$ K. The concentrations near the surface ($z=0.5$ mm) have been calculated using the procedures given in Ref. 15, while those *at* the surface have been estimated from these data using the methods A and B described in Sec. II A. T_g is the gas temperature, T_s is the experimental substrate temperature, and T_{ns} is the calculated temperature of the gas near ($z=0.5$ mm) the substrate. $[H]_s$ is a special case, and has been calculated using a detailed treatment of diffusion and surface reaction. $CH_2(s)$ refers to the singlet state, while $C_2(X)$ and $C_2(a)$ are the ground state and first excited state of C_2, respectively. The conditions for UNCD(MW) have been recalculated using a lower value for T_s. The total growth rate, G_{calc}, and crystal sizes, $\langle d \rangle$, are calculated using the equations in Ref. 15 while G_{KMC} is the growth rate calculated using the KMC model in this paper. Experimental values for G_{exp} and $\langle d \rangle$ are from the references given in Ref. 15.

Film type	SCD			MCD			NCD			UNCD			UNCD		
Reactor		MW			HF			HF			HF			MW	
T_s/K	973	973	973	1173	1173	1173	1173	1173	1173	1173	1173	1173	873	873	873
T_{ns}/K	1736			1267			1267			1145			1263		
z/mm, Method	0.5	0, A	0, B	0.5	0, A	0, B	0.5	0, A	0, B	0.5	0, A	0, B	0.5	0, A	0, B
Species, X	$[X]_{ns}$	$[X]_s$	$[X]_s$	$[X]_{ns}$	$[X]_s$	$[X]_s$	$[X]_{ns}$	$[X]_s$	$[X]_s$	$[X]_{ns}$	$[X]_s$	$[X]_s$	$[X]_{ns}$	$[X]_s$	$[X]_s$
H	3.38×10^{16}	3.38×10^{16}	3.38×10^{16}	1.85×10^{14}	1.85×10^{14}	1.85×10^{14}	1.52×10^{14}	1.52×10^{14}	1.52×10^{14}	3.00×10^{13}	3.00×10^{13}	3.00×10^{13}	4.31×10^{14}	4.31×10^{14}	4.31×10^{14}
CH_3	3.24×10^{13}	1.0×10^{13}	2.86×10^{13}	1.46×10^{13}	8.0×10^{12}	2.18×10^{13}	5.68×10^{13}	6.0×10^{13}	7.30×10^{13}	3.82×10^{13}	8.0×10^{12}	2.49×10^{13}	5.60×10^{11}	1.0×10^{12}	8.48×10^{12}
CH_2	1.06×10^{12}	1.0×10^{10}	5.65×10^{6}	2.72×10^{10}	1.0×10^{9}	4.50×10^{10}	8.12×10^{10}	2.0×10^{9}	1.00×10^{11}	1.55×10^{10}	1.0×10^{8}	2.76×10^{9}	2.31×10^{9}	1.0×10^{8}	6.13×10^{9}
$CH_2(s)$	5.97×10^{10}	1.0×10^{8}	6.38×10^{5}	3.66×10^{8}	1.0×10^{6}	6.90×10^{8}	1.14×10^{9}	5.0×10^{6}	1.00×10^{9}	5.62×10^{8}	1.0×10^{5}	6.97×10^{7}	6.08×10^{7}	1.0×10^{6}	9.46×10^{7}
CH	1.60×10^{11}	5.0×10^{8}	2.36×10^{3}	2.74×10^{8}	1.0×10^{6}	1.10×10^{9}	6.53×10^{8}	1.0×10^{6}	1.40×10^{9}	5.28×10^{7}	1.0×10^{4}	7.61×10^{6}	7.05×10^{8}	1.0×10^{7}	1.10×10^{9}
C	1.41×10^{12}	1.0×10^{10}	1.29×10^{4}	3.37×10^{9}	6.0×10^{8}	1.95×10^{10}	5.45×10^{9}	2.0×10^{9}	1.24×10^{10}	1.05×10^{7}	1.0×10^{4}	9.34×10^{5}	1.47×10^{11}	5.0×10^{9}	8.14×10^{9}
H_2	9.33×10^{17}	9.33×10^{17}	9.33×10^{17}	1.52×10^{17}	1.52×10^{17}	1.52×10^{17}	1.51×10^{17}	1.51×10^{17}	1.51×10^{17}	1.83×10^{17}	1.83×10^{17}	1.83×10^{17}	2.06×10^{16}	2.06×10^{16}	2.06×10^{16}
$C_2(a)$	4.19×10^{10}	1.0×10^{6}	2.66×10^{0}	6.57×10^{4}	1.0×10^{5}	2.25×10^{5}	1.74×10^{5}	2.0×10^{5}	1.76×10^{5}	2.49×10^{5}	1.0×10^{3}	1.11×10^{2}	1.16×10^{11}	1.0×10^{10}	6.58×10^{6}
$C_2(X)$	1.12×10^{10}	1.0×10^{5}	9.42×10^{-1}	1.41×10^{4}	4.0×10^{4}	1.50×10^{5}	5.40×10^{4}	6.0×10^{4}	1.33×10^{5}	1.49×10^{4}	1.0×10^{0}	1.11×10^{1}	4.93×10^{10}	5.0×10^{9}	3.4×10^{6}
C_2H_2	2.96×10^{16}	4.0×10^{17}	1.41×10^{16}	2.49×10^{11}	2.8×10^{11}	1.80×10^{11}	2.97×10^{12}	3.7×10^{12}	1.81×10^{12}	2.97×10^{13}	2.95×10^{13}	1.13×10^{13}	2.35×10^{15}	2.7×10^{15}	3.42×10^{15}
Ar										5.34×10^{17}			1.21×10^{18}		
$G_{calc}/(\mu m\ h^{-1})$	4.4	1.3	3.8	1.6	1.4	3.3	11.1	9.2	11.6	1.7	0.5	1.6	0.034	0.07	0.5
$G_{KMC}/(\mu m\ h^{-1})$	2.1	0.4	1.0	0.85	0.45	1.1	3.0	2.7	3.2	0.9	0.2	0.4	0.036	0.03	0.18
$\langle d \rangle$	2.1 cm	25 cm	3.1 cm	2.2 μm	7.04 μm	0.94 μm	94 nm	84 nm	57 nm	8.1 nm	185 nm	19 nm	12 mm	6 mm	84 μm
							Experimental values								
$G_{exp}/(\mu m\ h^{-1})$	3–4			0.35			~1.0			~0.1			~0.1		
$\langle d \rangle_{exp}$	>100 μm [a]			1–50 μm [b]			~100 nm			<10 nm			~15 nm		

[a]SCD over an area 2.5×2.5 mm^2 but with some round-shaped growth structures with heights up to 0.5 μm and widths ~100 μm.
[b]Depends on thickness.

Downloaded 10 Dec 2010 to 137.222.40.127. Redistribution subject to AIP license or copyright; see http://jap.aip.org/about/rights_and_permissions

TABLE II. Estimated values for g, s, and P for each CH_x species used in Eq. (3).

Species	g	s	P
CH_3	0.5	0.15	0.075
CH_2	0.6	0.2	0.12
CH	0.7	0.25	0.175
C	1.0	0.3	0.3

$$\bar{c} = (8RT_{ns}/\pi m_{CHx})^{1/2}, \tag{2}$$

where R is the gas constant, T_{ns} is the gas temperature near the surface (taken to be the same as T_s if the species concentrations are calculated for $z=0$), m_{CHx} is the relative molar mass of the species, and $[CH_x]_s$ is the concentration of the species with $x=0-3$ at the surface estimated using one of the two methods mentioned above. P is the probability of adsorption onto a radical site (i.e., the sticking probability). The value of P results from a combination of factors that reduce the reaction probability, such as a geometrical factor (g) due to unfavorable collision orientations and a steric-electronic factor (s), and we assume the two are independent, so that P is simply:

$$P = gs. \tag{3}$$

The factor s was previously estimated for CH_3 since it is known[27] from electronic-spin statistics that, on average, three collisions out of four will be on the triplet surface and will not lead to reaction at the high temperatures of diamond CVD. We also know that not all the surface radical sites will be accessible for adsorption, say ~50%–60%, giving an estimate for $s \sim 0.25 \times 0.6 = 0.15$. Taking a value for g of 0.5 gives an estimated value for P for CH_3 of ~0.075. In the absence of appropriate experimental data and a suitable method for their accurate calculation, the values of s and g for the other CH_x species have simply been estimated assuming that species with smaller radii are less sterically hindered (larger g) and have greater reaction probability (larger s). The estimates used are given in Table II.

C. Multiply-activated surface species

The second new consideration is that the CH_x species which adsorb onto the surface will not all form stable CH_2 bridging structures. Adsorbates other than CH_3 will first adsorb as 'activated' adducts, supporting one or more dangling bonds, with the degree of activation dependent upon the identity of the species adsorbed. As before, adsorbing CH_3 is modeled as an unactivated surface block, which is immobile and unreactive. Adsorbing CH_2 results in an activated surface block (i.e., it has one dangling bond), which is reactive and mobile, assuming there is an adjacent surface radical into which it can jump. Adsorbing CH leads to a doubly-activated block (i.e., two dangling bonds), which is highly reactive. Finally, adsorbing C atoms forms triply-activated blocks (three dangling bonds), which are more reactive still.

All of these activated surface species have three possible reaction pathways. One pathway is for the species and its dangling bonds to restructure locally on the surface forming a surface defect. This defect may become a renucleation site for the initiation of a new layer or for the creation of a new mismatched crystallite, resulting in polycrystalline growth. Modeling this pathway has been left for future work. The second pathway involves activation and deactivation of the various surface adsorbates. As before, unactivated CH_2 blocks can undergo an H-abstraction reaction with a rate given by

$$\text{Activation rate} = (k_1[H]_s)U, \tag{4}$$

while the rate of deactivating a surface radical site is

$$\text{Deactivation rate} = (k_2[H]_s + k_{-1}[H_2])A, \tag{5}$$

with U and A being the number of unactivated and activated surface blocks, respectively, and the rate constants, k_1, k_2, and k_{-1} given in Ref. 19. However, the activated blocks now have the possibility of undergoing a second H abstraction, and activating further to doubly-activated sites, or, further still, to triply-activated blocks. The reverse is also possible, the triply- and doubly-activated blocks can deactivate via sequential H-addition reactions. These reactions would obey rate equations of the same form as Eqs. (4) and (5), with the replacement of U and A, by the number of relevant activated or deactivated blocks, respectively.

D. Etching

The third possible pathway is removal of the activated species back to the gas phase via etching. Previously, we included an etching step for *all* the types of activated sp^3-bonded CH_x adsorbates[19] but only by the high-energy route of direct C–C bond cleavage. For $T_s = 1173$ K, and a C–C bond energy of ~350 kJ mol^{-1}, this gave a typical per site etching rate a factor of 1000 times slower than most other processes, suggesting that such etching processes are (almost) negligible. This is however incompatible with experimental evidence[28] whereby etching does occur under CVD conditions in the absence of methane. Recent etching experiments in our laboratory[29] using single-crystal diamond and H_2 microwave (MW) plasmas under similar conditions to that used for CVD showed that the average etch-rate of diamond (calculated by mass loss) over the whole surface is typically ~10% of the growth rate obtained for the same plasma conditions but with added CH_4. While the mechanism of this process is not yet clear, it should be included in our model. Thus, in the present study the etch-rate is chosen semi-empirically to reproduce the known ratio of deposition and etching rates. In terms of the KMC program, this is simply obtained by setting, as follows:

$$\text{overall etch rate} = 0.1 \times (CH_3 \text{ adsorption rate}). \tag{6}$$

Closer examination of the experimentally etched diamond surfaces[29] also showed that etching does not occur homogeneously across the surface. Etching appears to begin by the removal of an individual atom, probably a defect or impurity in the surface. The exposed sidewalls of this vacancy then etch back rapidly producing shallow, flat-bottomed, rectangular etch-pits many tens or hundreds of micrometers across, as shown in Fig. 2. Similar pits have also been seen when

Downloaded 10 Dec 2010 to 137.222.40.127. Redistribution subject to AIP license or copyright; see http://jap.aip.org/about/rights_and_permissions

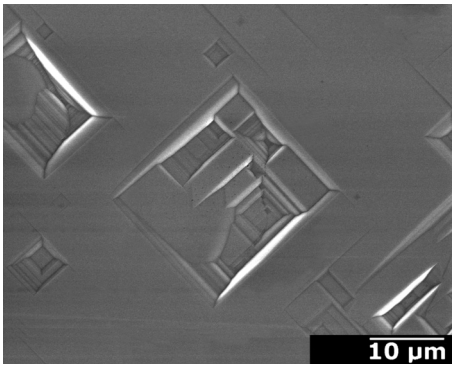

FIG. 2. Scanning electron micrograph of shallow, flat-bottomed, etch-pits formed when etching single-crystal diamond (100) in a 1 kW MW H_2 plasma at 150 Torr (Ref. 29).

etching single-crystal diamond in H_2/O_2 plasmas.[30] Thus, the lateral etch rate (etching back of step-edges) may be hundreds of times faster than the vertical etch rate.

Lateral step-edge etching has now been incorporated into the KMC program by adding a routine that, at every program step, first identifies the etchable blocks—which include activated sidewall blocks as well as activated adsorbed CH_2 groups- and then allows them to etch with a rate given by Eq. (6) multiplied by the total number of etchable blocks. Etching of terrace blocks on the diamond surface has not been included because the rate for this was considered negligible since it is ~1000 or more times slower than lateral step-edge etching.

E. Insertion reactions

Another new addition to the model is to consider the effects of insertion reactions by C_1 radical species. It has been calculated[31] that adsorbing C, CH, and CH_2(s) (singlet CH_2) can insert directly into a C–H surface bond with zero or small (20 kJ mol^{-1}) energy barrier. Thus, such insertion reactions, even to an *unactivated* site, may be rapid at typical CVD temperatures. The rate constants for these insertion reactions were calculated using an in-house transition-state-theory program as a function of T_s.[29] These were then fitted to the following mathematical expressions allowing the rate constants for insertion by C, CH, and CH_2(s), respectively, in $cm^3\ s^{-1}$, to be obtained for any value of T_s:

$$k_C = 8.59 \times 10^{-11} \exp(-2386/T_s), \tag{7}$$

$$\ln(k_{CH}) = (2 \times 10^6/T_s^2) - (18700/T_s) - 24.92, \tag{8}$$

$$k_{CH2(s)} \sim k_{CH}. \tag{9}$$

The insertion rate per surface site is then calculated by multiplying the rate constant by the concentration of the relevant species. Despite their much lower concentrations just above the surface compared to CH_3, the C_1 species may contribute to the growth mechanism because they can add to *all* of the surface sites whereas CH_3 can only add to the ~10% of sites that are activated. To quantify this, we added a routine to the KMC code that enables blocks that represent C, CH, and CH_2(s) species to adsorb onto *any* surface site, irrespective of whether the surface site was already activated. The newly added block will remain activated according to which species inserted: C produces a doubly-activated adduct, CH produces a singly-activated adduct, while CH_2(s) produces an unactivated adduct.

F. Surface radical migration

One important process neglected until now in most KMC models of diamond growth (see however Refs. 9–11), including our own, is migration of the surface radicals. This occurs when an adsorbed hydrogen jumps onto an adjacent carbon supporting a surface radical, leaving behind a new radical site. Thus, migration of H in one direction can be thought of as being equivalent to migration of a surface radical in the opposite direction. Unfortunately, there are complications in that the kinetics of H-atom migration depend on the direction of migration and the local surface geometry. Nevertheless, Frenklach and Skokov[10] have derived an Arrhenius expression for the rate constant for surface-radical (SR) migration averaged over the whole surface, as follows:

$$k_{SR} = 4.8 \times 10^{12} \exp(-155400/RT_s). \tag{10}$$

Putting $T_s \sim 1173$ K into this expression gives $k_{SR} \sim 6 \times 10^5\ s^{-1}$, which is ~200 times slower than the CH_2 hopping rate but $\sim 10^3$ times faster than the gas-surface reactions such as H abstraction/addition, and $\sim 10^5$ times faster than the CH_3 adsorption rate. Once k_{SR} is multiplied by the number of surface radicals to give the overall rate, the value obtained is sufficiently large that an average equilibrium distribution of radical sites can be assumed, and this is what has been implemented here. Thus, after every program step involving surface restructuring (etching, adsorption, insertion, CH_2 migration), the positions of the radical sites were randomized across the whole surface while ensuring that the proportion of activated and deactivated sites remained constant. We note that other QM/MM calculations[13] suggest that the barrier to H atom migration can be significantly higher than found in the work by Frenklach and Skokov, depending on the precise structure of the initial and final radical site, so that further refinements of the treatment of radical site migration may be needed in future.

G. Surface CH_2 migration

Surface migration along or across a dimer row is treated similarly to the previous model, with only the singly-activated adducts being allowed to migrate—but only if there is a suitable radical site in a neighboring position, i.e., if *both* the CH_2 is activated *and* there is a neighboring activated surface site to receive it, as required in the atomistic models of carbon migration.[13] We have chosen not to allow doubly- or triply-activated surface species to migrate because no mechanism has yet been reported in the literature for migration of these species, and also because their concentrations are sufficiently low that the effect of any migration processes are probably negligible. The significant change is that now we assume that the effective rate of CH_2 migration is not its Arrhenius hopping rate, but is limited by the lack of availability of an adjacent surface radical site into which the CH_2

Downloaded 10 Dec 2010 to 137.222.40.127. Redistribution subject to AIP license or copyright; see http://jap.aip.org/about/rights_and_permissions

TABLE III. Color codes for the blocks used in the KMC algorithm. "Yes" in the "Adsorption allowed?" column means that these blocks allow other blocks to attach on top of them, either by direct adsorption from the gas phase, migration, or "lemmings" processes.

Color code	Description	Mobile on surface?	Etchable?	Adsorption allowed?
Dark-blue	The subsurface bulk diamond lattice.	No	No	No
Grey	Hydrogenated (unactivated) surface layer.	No	No	No
Magenta	Dehydrogenated activated surface radical site (dangling bond).	No	No	Yes
Green	Hydrogenated (unactivated) adsorbed CH_2/CH_3 unit.	No	Yes	No
Red	Dehydrogenated activated adsorbed CH_2 unit.	Yes	Yes	Yes
Light-red	Doubly-activated adsorbed CH unit.	No	Yes	Yes
Yellow	Triply-activated adsorbed C unit.	No	Yes	Yes

may hop. The rate at which adjacent radical sites become available is governed initially by the equilibrium between H abstraction and H addition rates, and then by a combination of the H abstraction rate and rate of SR migration. For most CVD conditions, the SR migration rate is much faster than that of H abstraction, the exception being under the high-power, higher pressure conditions used for SCD growth where the two rates can become comparable. To account for this, the effective CH_2 migration rate in the KMC model is simply made equal to the faster of these two rates.

We have continued to use the "lemmings" scenario as the default process that occurs when migrating blocks encounter the top of a step-edge. This scenario allows the blocks to migrate off the top of a step-edge at the same rate as migration on the flat, so long as there is a radical site adjacent to the bottom of the step-edge upon which the block can land.

H. β-scission

β-scission is also modeled as before, with the rate being given simply by $k_\beta B$, where k_β is the rate constant for the β-scission reaction[19] and B the number of *activated* 2-block columns present on the surface at any one time. In this case, we have allowed β-scission to occur if the topmost block is singly-, doubly-, or triply-activated, although this choice makes little difference because, for most growth conditions, β-scission makes only a minor contribution to the overall deposition process.

III. GROWTH PARAMETERS

In order to test the predictions of the KMC model over the range of deposition conditions used for growth of different types of diamond we require knowledge of the concentrations of atomic H, CH_3 and the remainder of the other C_1 hydrocarbon radicals (C, CH, and CH_2) at the growing diamond surface, all as a function of deposition conditions (pressure, T_s, etc.). These parameters have been calculated using the model described in Ref. 15 for the gas mixtures and conditions used experimentally to deposit SCD, MCD, NCD, and UNCD in both hot filament and microwave (MW) reactors, allowing the identities and concentrations of the gaseous species near the diamond surface in each of these situations to be estimated. These data were then analyzed using the two methods described in Sec. II A to estimate the concentrations $[X]_s$ of all these species *at* the surface ($z=0$). The concentrations for a sub-set of the most abundant and relevant species are given in Table I. Based on our previous growth model these data were used to calculate the expected growth rate, G, and average crystal size, $\langle d \rangle$, for each type of diamond film, and the results agreed reasonably well with experimental findings. The exception was for UNCD grown in a MW reactor, where the predicted $\langle d \rangle$ was incorrect by many orders of magnitude. Until now, the origin of this discrepancy remained unclear, and we assumed that there must be some factor in the modeling of either the gas phase chemistry or the gas-surface interactions for UNCD(MW) conditions that was not accounted for. We shall return to this point later in Sec. V.

IV. THE KMC MODEL

The original model for the KMC program is given in Refs. 17 and 18, and so only a brief description will be given here. The (100) diamond lattice is represented in only 2 dimensions, as a cross-section. Each C atom is represented by a square block within the lattice. New blocks are allowed to adsorb onto random (but previously activated) positions on this surface, after which they may adsorb, migrate across the surface, be etched away, or add to the lattice, with each process having a rate generated at each step of the program based upon the current occupancy of the lattice array. These new blocks represent generic C_1 adsorbing units, which are usually CH_3 but may now include C, CH, CH_2, or CH_2(s).

Color-coding the blocks within the array is used to represent different "types" of carbon bonding and for ease of description (see Table III). Carbons that are fully bonded into the bulk diamond lattice are colored dark-blue whereas hydrogenated carbons that form the surface layer are colored gray. A surface radical site is colored magenta, and is created as a result of a gray block being "activated" by a successful H abstraction. Green blocks are used to represent pendant CH_3 groups or bonded CH_2 structures that bridge along or across the rows of the dimer pairs on the reconstructed (100) surface. These are considered to be immobile, although they may rapidly interconvert between the CH_3 and CH_2 forms as a result of H addition/abstraction reactions. An immobile

Downloaded 10 Dec 2010 to 137.222.40.127. Redistribution subject to AIP license or copyright; see http://jap.aip.org/about/rights_and_permissions

green block can become activated following a successful H-abstraction reaction. Such activated blocks are colored red, and are allowed to migrate to a neighboring block, so long as there is a SR site (magenta) present there. Red blocks can be further activated by successive H-abstraction reactions to doubly-activated (light-red) or triply-activated (yellow) blocks. These, in turn, can be deactivated by successive H-addition reactions. All activated adsorbates can be etched from the substrate, as can activated step-edge blocks (magentas with a vacancy to one side). β-scission can remove any two-block columns that have an activated top-block.

The grid has a maximum size of 600×400. At the start of the program, a flat horizontal surface of gray blocks is defined at the bottom of the screen to represent the surface of a single-crystal diamond substrate. The program proceeds by generating a random number, N $(0 \leq N < 1)$, so that at each simulation step a process is chosen with a probability proportional to its rate. The randomly chosen process is carried out, along with any consequences, and a new list of possible processes is generated ready for the next random number comparison. The processes involved are:

- *Activation of a surface site*: gray block becomes magenta.
- *Deactivation of an activated surface site*: magenta block becomes gray.
- *Adsorption of a CH_x species onto a radical site*: a new green, red, light-red, or yellow block is chosen at random based on the relative abundances of CH_3, CH_2, CH, and C, respectively, and adds on top of an existing activated site, which may be magenta, red, light-red or yellow, again, chosen at random based on their relative abundances. The underlying block then becomes dark-blue as it is now considered to be bulk diamond.
- *Insertion of a CH_x $(x<3)$ species into a nonradical site*: a new green, red, or light-red block is chosen at random based on the relative abundances of CH_2(s), CH, and C, respectively, and adds on top of an existing gray surface site chosen at random. The underlying gray block then becomes dark-blue.
- *Etching of adsorbates*: a red, light-red, or yellow block is removed from the surface and forgotten, the newly exposed underlying block becomes magenta.
- *Etching of step-edges*: a magenta sidewall block is removed from the surface and forgotten, the newly exposed underlying block becomes magenta.
- *Activation of adsorbed groups*: green blocks become red, reds become light-red, light-reds become yellow.
- *Deactivation of adsorbed groups*: yellow blocks become light-red, light-reds become red, reds become green.
- *CH_2 Migration*: a red block hops left or right one position, so long as there is a magenta available to jump into—if migration occurs, the block jumps to the neighboring site (and remains red) and the magenta becomes dark-blue. The site previously occupied by the red now becomes magenta.
- *Addition to the lattice*: either via an Eley–Rideal-type process—an adsorbing block lands immediately adjacent to a step-edge and fuses to the lattice and turns gray; or a Langmuir-Hinshelwood-type (LH) process—a migrating red block meets a step-edge, fuses to the lattice and turns gray.
- *Sub-surface layer*: once a block is no longer part of the surface layer it turns dark-blue.
- *β-scission*: any two-block pillars with activated top-blocks are removed and the exposed underlying block becomes magenta.
- *CH_2 migration off the top of step-edges*: using the "lemmings" scenario, red blocks can migrate off a step-edge and land in the bottom corner so long as the surface block beneath is activated, i.e., magenta, whereupon the red block fuses to the lattice and becomes gray.
- *Migration of surface radicals*: following any process that changes the block positions (etching, migration, β-scission, adsorption, and insertion) all the magenta and gray blocks are combined and randomized, such that some of the greys become magentas and vice versa, while ensuring that the magenta:gray ratio remains constant.

The program ran until it was stopped manually or until a preset number of layers (typically 150–300 to provide statistical invariance) had formed, at which point the data were saved. Depending upon the input parameters for the various events, the program took from a few minutes to a few days to simulate growth of 300 layers on a Pentium-4 PC. At each step the time taken, t_{new}, was updated according to

$$t_{new} = t_{old} - \ln(N)/\Sigma R, \tag{11}$$

where t_{old} is the cumulative time up to the previous step, N is a new random number $(0 \leq N < 1)$, and ΣR is the sum of the rates of all possible processes.[32] Typically 10^9 steps were required to simulate 150 layers of growth, with the total growth time simulated being around 10–50 s depending on conditions used. The growth rate was calculated from knowledge of the number of layers of diamond that grew in this time, and the average C–C distance along a (100) diamond face (i.e., one block ~ 0.0892 nm).

V. RESULTS AND DISCUSSION

Table I shows that there is good agreement (factor of ~ 3) between G_{KMC}, the growth rates calculated using the KMC program (using both methods to estimate the species concentration at the surface), G_{calc}, the growth rates calculated using the growth model outlined in Ref. 15, and G_{exp}, the experimental growth rates, despite the rather approximate nature of the estimation of the g and s parameters used in Eq. (3) which determine the absolute value of G_{KMC}. It is important to recall that the growth rate is for the total film thickness, irrespective of diamond quality or composition. The predicted growth rates for SCD and MCD are $\sim 0.4-1.1$ μm h^{-1}, while NCD has a higher growth rate of ~ 3 μm h^{-1}, mainly due to the increased CH_4 concentration. However, this film exhibited cauliflower morphology, and thus a significant fraction of its composition would include

Downloaded 10 Dec 2010 to 137.222.40.127. Redistribution subject to AIP license or copyright; see http://jap.aip.org/about/rights_and_permissions

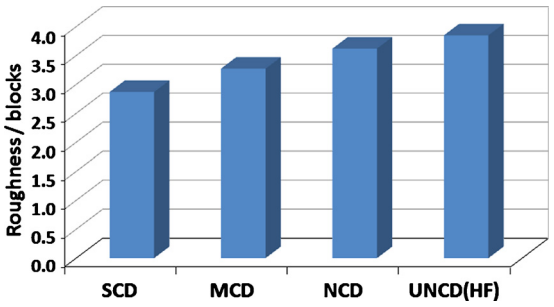

FIG. 3. (Color online) The rms roughness of the various diamond films following growth of 150 layers. A value of rms roughness of, say, two blocks for growth of 150 layers means the surface had a mean height of 150 ± 2 blocks over a width of 300 blocks. Data are calculated for species concentrations at the surface that were estimated using method B. Method A produced roughness values and trends very similar to these.

nondiamond carbon. UNCD grown in a HF reactor also has a low growth rate (0.2–0.4 μm h^{-1}), consistent with its reduced substrate temperature during growth.

Figure 3 shows the root-mean-square (rms) roughness of the diamond surface for the different film types following growth of 150 layers. Since renucleation and grain formation is not yet included in the model, this roughness value reflects the intrinsic atomic-scale roughness that results from the random nature of CVD growth. As expected, SCD is relatively smooth on this scale [Fig. 4(a)], while NCD and UNCD films are much rougher [Fig. 4(b)].

The average surface-diffusion length, ℓ, is defined as the mean distance (measured in a straight line from its initial adsorption site) that a migrating species has traveled when its migration is permanently terminated by processes such as etching, attachment to the lattice, etc. Figure 5 shows ℓ plotted for each of the different diamond growth conditions. As

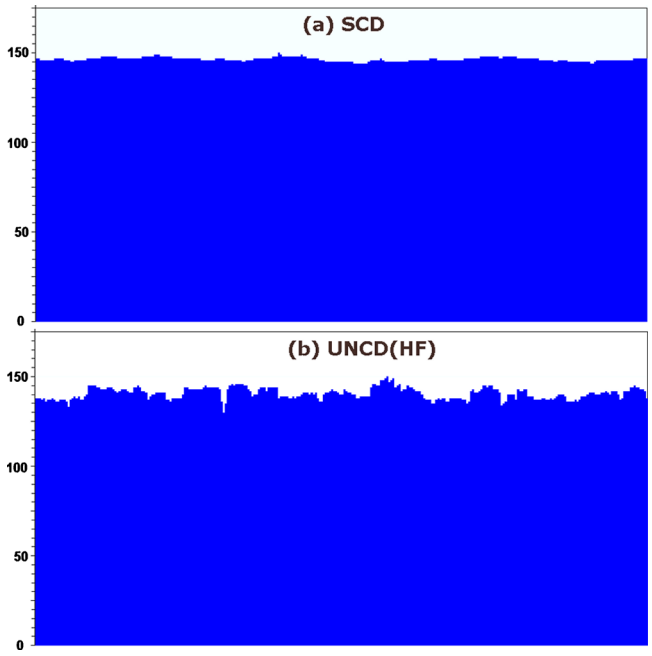

FIG. 4. (Color online) Simulated cross-sections of (100) diamond growth using (a) SCD (MW reactor) and (b) UNCD (HF reactor) conditions, showing their relative surface roughness. The scale is 150 blocks (equivalent to carbon atoms) high by 300 blocks wide.

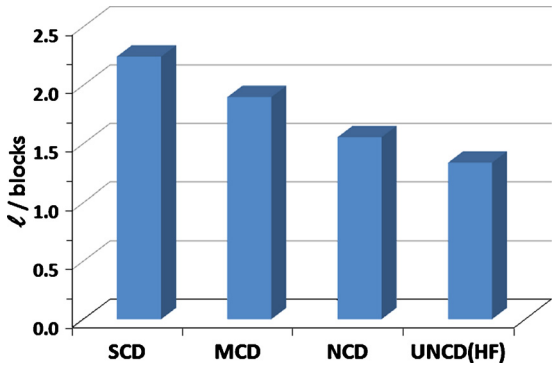

FIG. 5. (Color online) Average surface diffusion length, ℓ, calculated for the different diamond growth conditions. Methods A and B produced similar results.

expected, ℓ decreases from a value of ~2.2 sites for SCD growth to ~1.25 sites for UNCD. This is evidence that migration is a key mechanism by which the surface becomes smoother. Figure 6 emphasizes this idea, as it shows that the percentage of the total growth that results from ER processes (direct adsorption/addition) increases from a low value of ~28% for SCD to a much higher value of 48% for UNCD. Similarly, the percentage growth that results from LH processes (migration then addition) is very high for SCD (70%), dropping to ~46% for UNCD. Thus, migration-driven LH processes dominate for the smoother films (SCD, MCD), while direct-adsorption-driven ER processes dominate for the rougher films (UNCD).

Another insight into the growth mechanism is revealed by Fig. 7, which shows the average number of migration hops, n, made by the surface species for the different growth conditions. For UNCD, NCD, and MCD, n is of the order of several hundred, and increases as the migration rate increases. This is consistent with our previous findings[19] (although the n values are now approximately ten times smaller than those calculated before due to the inclusion of the surface radical migration mechanism) and can be explained by migrating species hopping back and forth between two adjacent empty surface sites. Thus, for these conditions n is very large, while ℓ remains low at <2 (see Fig. 5). However, for SCD conditions n drops significantly to ~130, and this coincides with the films becoming smoother, as mentioned

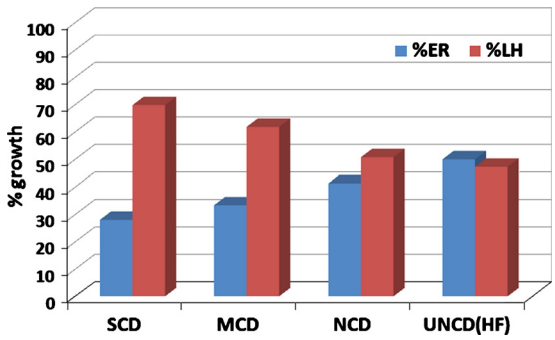

FIG. 6. (Color online) Percentage of total diamond growth that resulted from Eley–Rideal-type (left, blue) and Langmuir–Hinshelwood-type (right, red) processes for the different diamond growth conditions. The small difference between ER%+LH% and 100% is due to growth by other mechanisms such as insertions. Methods A and B produced similar results.

Downloaded 10 Dec 2010 to 137.222.40.127. Redistribution subject to AIP license or copyright; see http://jap.aip.org/about/rights_and_permissions

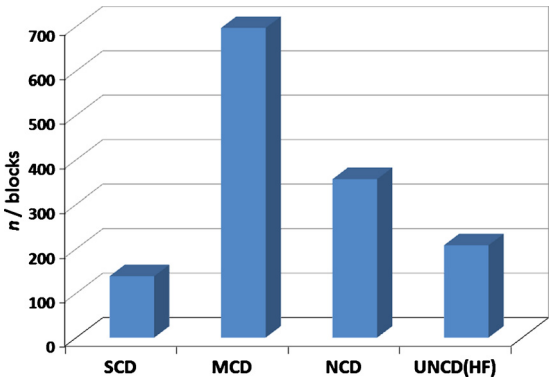

FIG. 7. (Color online) The average number of jumps, n, made by species migrating on the surface for each of the different diamond growth conditions. Methods A and B produced similar results.

above. Therefore, it appears that for these smoother films migration is now able to proceed beyond the immediate neighbors to sites two or three atoms distant. The fraction of available surface radical sites, F, changes from ~4% to 10% for the different growth conditions, but not in a monotonic fashion. Thus, the steady-state number of surface radical sites cannot account for these apparent differences in migration behavior.

Further clues can be obtained from Fig. 8, which shows the relative rates of surface H abstraction, and migration rates of radicals and CH_2 groups on the surface. For all growth conditions the rates of CH_2 migration are roughly similar, as are the rates of SR migration except for the case of SCD where the rate is markedly reduced due to the lower T_s. For MCD, NCD, and UNCD growth conditions, the rate of CH_2 migration is greater than that of H abstraction by more than two orders of magnitude. In these cases, CH_2 migration is limited by the rate at which existing surface radicals migrate across the surface, which is a function of $[H]_s$ and especially T_s. However, for SCD conditions, the H-abstraction rate is now much larger than the SR migration rate, and H abstraction now governs the rate of CH_2 migration. In this case the rapid rate of activation of the CH_2 surface groups, not the surface radicals, is key to their increased migration rate and, therefore, to the overall growth process.

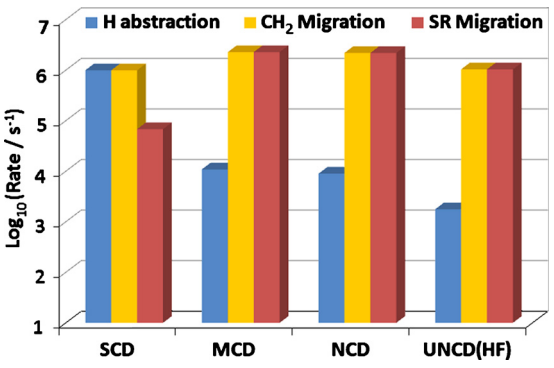

FIG. 8. (Color online) Rates of H abstraction (left, blue), CH_2 surface-migration (center, orange) and surface-radical migration (right, red) plotted on a common-logarithmic scale for the different diamond growth conditions. Methods A and B produced similar results.

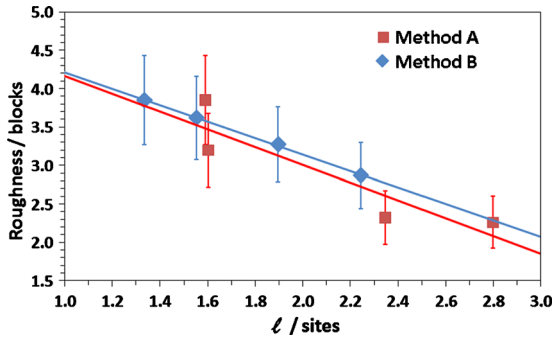

FIG. 9. (Color online) The rms surface roughness for the different diamond deposition conditions plotted against the surface diffusion length, ℓ. The two sets of data are for the two different methods used to estimate the species concentrations at the surface described in Sec. II A: Method A (red squares) and method B (blue diamonds). There was typically ~15% run-to-run variation in the calculated values of roughness due to the random nature of the Monte Carlo procedure and these have been indicated as error bars.

We have already inferred from Figs. 3 and 5 that surface roughness is related to ℓ, and this can be quantified by plotting in Fig. 9 a graph of rms roughness against ℓ for the sets of data obtained using the two methods for estimation of the species concentrations at the surface. This graph suggests a linear dependence of the approximate form: Roughness $=\ell_0 - k\ell$, where ℓ_0 is the 'intrinsic roughness' that would be obtained during diamond deposition if surface diffusion did not occur. In other words, ℓ_0 can be thought of as the roughness value resulting from 100% ER growth. Taking the average for the fitted gradients and intercepts for the two sets of data we find: $\ell_0 \sim 5$ blocks and $k \sim 1.1$. Conversely, assuming it is valid to extrapolate the straight lines in Fig. 9 to larger ℓ, and using the average values for k and ℓ_0 above, the equation predicts a perfectly flat surface (roughness=0) for a diffusion length of approximately four to five sites.

Previously, for MCD conditions, we found that β-scission reactions usually play only a small part in smoothing the film surface.[19] Fig. 10 shows the relative importance of β-scission for the different growth conditions. As expected, β-scission remains a minority process for SCD conditions, where the migration rates are high enough that blocks can migrate down off the top of two-block pillars faster than they can be removed by β-scission. However,

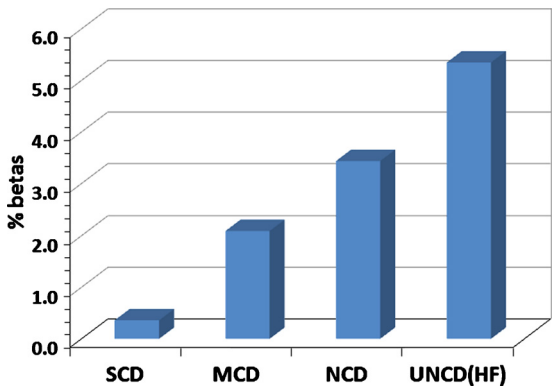

FIG. 10. (Color online) Percentage of carbons added to the surface subsequently removed by a β-scission reaction for the different diamond growth conditions. Methods A and B produced similar results.

Downloaded 10 Dec 2010 to 137.222.40.127. Redistribution subject to AIP license or copyright; see http://jap.aip.org/about/rights_and_permissions

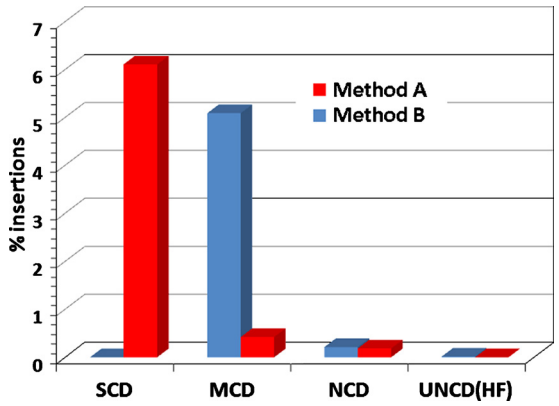

FIG. 11. (Color online) Percentage contribution to growth by C_1 insertion processes for the different diamond deposition conditions. Data are for method A (right, red) and method B (left, blue).

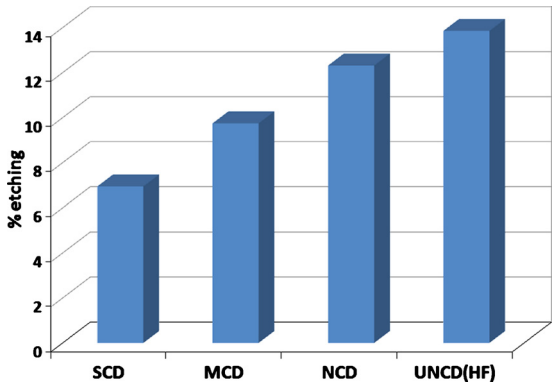

FIG. 12. (Color online) Percentage of carbons which are etched from the diamond surface for the different diamond deposition conditions. Methods A and B produced similar results.

when the migration rates are slower, as in the case of MCD, NCD, and UNCD (or at low T_s), β-scission starts to become a significant loss mechanism for C species, and is responsible for removing between ~2%–5% of the surface carbons as well as helping to smooth the surface.

Figure 11 shows the percentage contribution to the growth made by the C_1 insertion processes for each of the diamond deposition conditions. Although insertion by all C_1 species is included, C atoms account for the majority (99%) of these reactions due to their high abundance relative to the other C_1 species and high reaction probability, P (see Table II). It can be seen that, as expected, for most conditions such insertion reactions play only a small role in growth, typically contributing <0.5% of the carbon atoms in the diamond lattice. The two cases (SCD and MCD) where there is an apparently large contribution are probably misleading, as the two methods (A and B) used to determine the species concentrations at the surface in each case produce contradictory values. When method A predicts a ~5%–6% contribution, method B predicts <0.5%, and vice versa. This contradiction highlights the need to develop a more accurate method to estimate these surface concentrations from existing models of the gas-phase chemistry. Perhaps, also, different methods of estimating these concentrations may be more accurate or more applicable than others for different growth systems (e.g., hot filament or MW plasma) and/or growth regimes. Nevertheless, the values in Fig. 11 suggest that C_1 insertion reactions contribute, at most, 6% to the growth, but more likely contribute much less than this. As a result, insertion reactions can usually be neglected when considering the broader aspects of diamond growth, although they may still play an important role in defect formation and renucleation.

Figure 12 shows the percentage of adsorbed carbons that were subsequently removed from the surface by etching. This figure includes direct etching of both the migrating CH_2 groups and sidewall etching. The values of 6%–13% are consistent with the experimental findings mentioned earlier, which is the expected result of the fitting factor of 0.1 used in Eq. (6). Figure 12 shows etching becomes less common with increasing quality of diamond film. This is because we have not included any dependence of etching upon growth parameters (e.g., T_s or $[H]_s$), and therefore the etch rate simply reflects the roughness of the surface. When the surface is smoother (as for SCD) there are less sidewalls to attack and the etch-rate is reduced; when the surface is rougher (e.g., UNCD) there are many more sidewalls and step-edges to attack and a corresponding increase in etch-rate.

The analysis we have presented until now has deliberately omitted the data for UNCD grown in a MW system (see Table I, last column), because almost always the UNCD(MW) data did not fit the trend and/or gave anomalous behavior. Indeed, we commented previously[15] that the calculated gas phase concentrations for UNCD(MW) appeared inconsistent with our general diamond growth mechanism, and that the value for $\langle d \rangle$ calculated from the use of these concentrations predicted grain sizes of the order of millimeters rather than nm.

We previously had no clear explanation for this discrepancy, although we suggested that secondary growth processes that are not included in the growth model might be significant. These could be factors such as unknown specific features of the C-atom growth mechanism, or a possible increased rate of renucleation due to other hydrocarbon species (e.g., C_2, C_2H, C_3, and C_3H). Using the UNCD(MW) values from Table I, method A, as inputs in the KMC program predicts values for the rms surface roughness (3.3), n (~640) and ℓ (1.5), which are more consistent with SCD growth than UNCD, although the predicted growth rate (0.03 μm h^{-1}), though small, is realistic. These values suggest that the discrepancy lies in the values for the gas phase concentrations, and not in the growth or KMC models. One obvious difference between the gas chemistry in UNCD(MW) growth conditions and all the other (MW or HF) conditions is in the number of observed gas phase particulates. There are many reports that the plasmas used for UNCD(MW) growth produce a significant number of solid particulates, with sizes ranging from 10^{-9} to 10^{-5} m. The composition and nature of the particulates in these so-called "dusty" plasmas is not certain, but they are believed to be soot (amorphous or sp^2 carbon), polyaromatic hydrocarbons (PAHs),[33] fullerenes, or even nanodiamonds.[34] They are believed to be formed by homogeneous nucleation in the cooler parts of the chamber, such as around the periphery of the plasma ball, but can diffuse around the chamber and re-enter

Downloaded 10 Dec 2010 to 137.222.40.127. Redistribution subject to AIP license or copyright; see http://jap.aip.org/about/rights_and_permissions

the plasma ball whereupon they contribute to and perturb the chemical environment. Indeed, we have previously used the presence of such particulates in the plasma ball to estimate the gas temperature, as they absorb energy via collisions with other gas phase species, which they then emit as black-body radiation.[35]

The effect of particulates on UNCD(MW) deposition conditions has not been intensively studied to date. Despite the apparent similarity in conditions, far fewer particulates have been observed under UNCD(HF) conditions than UNCD(MW). There is a much smaller volume of hot gas present in a HF system (a few cubic millimeters at most) compared to that in a MW system ($\sim$100 cm^3). Also, in HFCVD reactors the temperatures are generally lower, and methane conversion to C_2H_2 and heavy hydrocarbons (probable precursors of the particulates) is reduced. Under UNCD(MW) conditions these particulates may reduce the electron concentration because particles in the plasma can accumulate large negative charge and increase the electron temperature,[34] and this may affect the heat balance in the plasma. But another major factor may be the large surface area that is now present *within* the hot plasma region and which is available for gas-surface reactions.

The soot particle nucleation rate has been estimated[36] at $\sim 10^{11}$ nuclei cm^{-3} h^{-1} for $T_g < 1500$ K in an $Ar/H_2/CH_4$ (97:2:1) plasma. If such high rates could provide significant particulate concentrations (say $\sim 10^8$–10^9 cm^{-3}) than there will be an additional large surface (with area up to dozens of square centimeters for particulate diameters of $\sim$10–100 nm) in the outer plasma regions during UNCD(MW) growth. Various gas-surface reactions (e.g., H atom recombination, loss of hydrocarbon species, ions) on such a large surface area may drastically change the plasma-chemistry and species concentrations. Our first calculations involving the heterogeneous recombination of H atoms showed that this produced a serious drop in H atom concentration, but that this did not disturb significantly the $[H]_s/[CH_x]_s$ ($x=0$–3) ratio, and, moreover, failed to provide the relevant conditions for UNCD growth.

The particulates are subject to diffusion and convection within the chamber, and often deposit on many cold surfaces in the chamber, including the walls, viewport, and quartz window. There has been speculation that these particulates may also land onto the surface of the substrate and either help to nucleate diamond growth, or even be responsible for nanodiamond growth.[37] However, we have never found any evidence for the particulates depositing onto the hot substrate surface, although we cannot exclude that they may have deposited and embedded in growing film, as has been observed for SiC nanocrystalline film growth at substrate temperatures $\sim$350 °C.[38]

In favor of this mechanism we note that the gas-phase conditions and reaction mechanisms in the peripheral shell of the plasma region (the location where the particulates are commonly observed[33]) are replicated[39] in the thin layer (few millimeters) above the substrate. (This was the assumption inherent in one of the methods described earlier to estimate the concentration of species at the surface). Thus, intensive formation of nanoparticles within this boundary layer and at the substrate surface, e.g., from C_2H_x, heavy hydrocarbons C_xH_y (via the hydrogen-abstraction carbon-addition (HACA) mechanism[40]), and/or charged species, is quite probable, and may contribute to or be an essential part of the UNCD(MW) deposition mechanism in conventional $Ar/H_2/CH_4$ MW plasma mixtures. The role of various processes involving charged species, i.e., deposition of positive ions $C_xH_y^+$, the coagulation of negative particles to form charged clusters which have been described[41] and observed in low-temperature plasmas[42,43] needs to be studied in the context of UNCD growth.

VI. CONCLUSIONS

Although defect formation and renucleation are not yet included in the growth model, the simple 1D KMC program predicts reasonably successfully the growth rates and morphology trends for diamond films varying from UNCD to SCD. The intrinsic surface roughness has been shown to be directly related to the surface diffusion length, ℓ. This is determined by the instantaneous availability of adjacent surface radical sites into which the migrating species can jump, which, in turn, is governed by the rates of surface-H abstraction and of SR migration, both of which are ultimately determined by the substrate temperature and the H-atom concentration at the surface. When these two rates are low, surface species simply hop back and forth between two adjacent sites many times, but never travel more than one or two sites from their original adsorption position. This leads to predominantly ER growth with rough surfaces, consistent with NCD or UNCD films. Conversely, when the rate of H abstraction and/or the rate of SR migration become high enough, the migrating species can hop more than one site and begin to sample more of the surrounding area. This leads to predominantly LH growth, smoother surfaces, and MCD or SCD films. The roughness values presented here are on the atomic scale, and we predict that a maximum rms roughness of five atoms would occur for $\ell=0$, i.e., for pure ER growth. Conversely, atomically smooth films over very large areas could be produced for $\ell \sim 5$, but to achieve this would require an idealized system that could produce a very high ratio of $[H]_s/[CH_x]_s$ ($x=0$–3) at the surface. Although renucleation and defect formation would modify this value, these findings nevertheless highlight the notion that for high quality SCD deposition we require extremely high H atom concentrations.

An interesting conclusion from these studies is that despite the very different gas mixtures, temperatures and process conditions, used to deposit the four types of diamond, the growth process is dominated by only two species. The flux of CH_3 to the surface governs the growth rate while the flux of atomic H controls the rate of all surface reactions, including etch rate and mobility of adsorbed CH_2 species, and hence surface roughness. The role of all other hydrocarbon radicals (C, CH, CH_2, C_2, etc.) in the overall growth process is minimal due to their negligible concentrations at the surface compared to that of CH_3. The fact that there appears to be no correlation between the relative contribution of insertion reactions to overall growth and crystal size, and

Downloaded 10 Dec 2010 to 137.222.40.127. Redistribution subject to AIP license or copyright; see http://jap.aip.org/about/rights_and_permissions

that this contribution is minimal in all cases, suggests that insertion reactions are not a significant route to surface-defect formation and to subsequent renucleation events. Thus, the renucleation events that produce smaller grain sizes must arise from other mechanisms, such as surface restructuring at biradical sites or misaligned bonding of the migrating CH_2 species to step-edges. Identifying the cause of surface defects, and also which of these defects are the ones that lead to renucleation[26] will be a vital next step if we are to progress to model polycrystalline films.

Nanoparticle formation above and at the substrate surface from heavy hydrocarbons C_xH_y and/or charged species is proposed as being important during UNCD deposition in $Ar/H_2/CH_4$ MW-plasma mixtures. The effects of these nanoparticles upon gas composition, reactions and temperatures require further study.

In future work we shall explore these implications further and investigate the effect of defect formation and renucleation upon the predicted growth rates and surface morphology. Converting the program to a full 2D geometry will also help to shed light upon aspects of the growth that depend more critically upon the exact local surface morphology, such as the shape and size of the critical nucleus, kinks, and protrusions in step-edges, attachment of migrating block to inside and outside corners, migration down risers, and possible void formation.

ACKNOWLEDGMENTS

The authors wish to thank Mike Ashfold, Neil Fox, and Keith Rosser for useful discussions and suggestions. The Bristol-Moscow collaboration is supported by a Royal Society Joint Project Grant, and Y.A.M. acknowledges support from the RF Government for Key Science, Schools Grant No. 3322.2010.2.

[1]P. W. May, Science **319**, 1490 (2008).
[2]P. W. May, Philos. Trans. R. Soc. London, Ser. A **358**, 473 (2000).
[3]P. W. May, in *Carbon Based Nanomaterials*, edited by N. Ali, A. Öchsner, and W. Ahmed, (Trans Tech, Switzerland, 2010), Chap. 6, pp. 145–176.
[4]D. G. Goodwin and J. E. Butler, in *Handbook of Industrial Diamonds and Diamond Films*, edited by M. A. Prelas, G. Popovici, and L. K. Bigelow (Marcel Dekker, New York, 1998).
[5]S. J. Harris, Appl. Phys. Lett. **56**, 2298 (1990).
[6]J. E. Butler, R. L. Woodin, L. M. Brown, and P. Fallon, Philos. Trans. R. Soc. London **342**, 209 (1993).
[7]K. Larsson, Phys. Rev. B **56**, 15452 (1997).
[8]H. Kawarada, H. Sasaki, and A. Sato, Phys. Rev. B **52**, 11351 (1995).
[9]S. Skokov, B. Weiner, M. Frenklach, T. Frauenheim, and M. Sternberg, Phys. Rev. B **52**, 5426 (1995).
[10]M. Frenklach and S. Skokov, J. Phys. Chem. B **101**, 3025 (1997).
[11]M. Frenklach, S. Skokov, and B. Wiener, Nature (London) **372**, 535 (1994).
[12]W. J. P. van Enckevort, G. Janssen, W. Vollenberg, J. J. Schermer, L. J. Giling, and M. Seal, Diamond Relat. Mater. **2**, 997 (1993).
[13]A. Cheesman, J. N. Harvey, and M. N. R. Ashfold, J. Phys. Chem. A **112**, 11436 (2008).
[14]K. Larsson and J.-O. Carlsson, Phys. Status Solidi A **186**, 319 (2001).
[15]P. W. May and Yu. A. Mankelevich, J. Phys. Chem. C **112**, 12432 (2008).
[16]A. Netto and M. Frenklach, Diamond Relat. Mater. **14**, 1630 (2005).
[17]P. W. May, N. L. Allan, J. C. Richley, M. N. R. Ashfold, and Yu. A. Mankelevich, J. Phys.: Condens. Matter **21**, 364203 (2009).
[18]P. W. May, N. L. Allan, M. N. R. Ashfold, J. C. Richley, and Yu. A. Mankelevich, Diamond Relat. Mater. **19**, 389 (2010).
[19]P. W. May, J. N. Harvey, N. L. Allan, J. C. Richley, and Yu. A. Mankelevich, J. Appl. Phys. **108**, 014905 (2010).
[20]J. C. Richley, J. N. Harvey, and M. N. R. Ashfold, in *Diamond Electronics and Bioelectronics—Fundamentals to Applications III*, MRS Symposia Proceedings No. 1203, edited by P. Bergonzo, J. E. Butler, R. B. Jackman, K. P. Loh, and M. Nesládek (Materials Research Society, Pittsburgh, 2010), pp. J17–J32.
[21]Y. A. Mankelevich, A. T. Rakhimov, and N. V. Suetin, Diamond Relat. Mater. **5**, 888 (1996).
[22]Yu. A. Mankelevich, M. N. R. Ashfold, and J. Ma, J. Appl. Phys. **104**, 113304 (2008).
[23]See supplementary material at http://dx.doi.org/10.1063/1.3516498 for the gas-phase concentrations calculated for a selected subset of the species near the growing diamond surface during CVD for SCD, MCD, NCD, and UNCD(HF) growth conditions.
[24]A. D. Terekhov and E. N. Frolova, J. Appl. Mech. Tech. Phys. **13**, 582 (1974).
[25]M. Eckert, E. Neyts, and A. Bogaerts, Cryst. Eng. Comm. **11**, 1597 (2009).
[26]M. Eckert, E. Neyts, and A. Bogaerts, Cryst. Growth Des. **10**, 3005 (2010).
[27]S. J. Klippenstein, Y. Georgievskii, and L. B. Harding, Phys. Chem. Chem. Phys. **8**, 1133 (2006).
[28]R. E. Rawles, S. F. Komarov, R. Gat, W. G. Morris, J. B. Hudson, and M. P. D'Evelyn, Diamond Relat. Mater. **6**, 791 (1997).
[29]J. C. Richley, Ph.D. thesis, University of Bristol (in preparation).
[30]J. Achard, F. Silva, O. Brinza, X. Bonnin, V. Milne, R. Issaoui, M. Kasu, and A. Gicquel, Phys. Status Solidi A **206**, 1949 (2009).
[31]J. C. Richley, J. N. Harvey, and M. N. R. Ashfold, J. Phys. Chem. A **113**, 11416 (2009).
[32]A. B. Bortz, M. H. Kalos, and J. L. Lebowitz, J. Comput. Phys. **17**, 10 (1975).
[33]K. Hassouni, F. Mohasseb, F. Bénédic, G. Lombardi, and A. Gicquel, Pure Appl. Chem. **78**, 1127 (2006).
[34]T. Gries, L. Vandenbulcke, J. N. Rouzaud, and S. de Persis, Plasma Sources Sci. Technol. **19**, 025015 (2010).
[35]O. J. L. Fox, J. Ma, P. W. May, M. N. R. Ashfold, and Yu. A. Mankelevich, Diamond Relat. Mater. **18**, 750 (2009).
[36]N. Aggadi, C. Arnas, F. Bénédic, C. Dominique, X. Duten, F. Silva, K. Hassouni, and D. M. Gruen, Diamond Relat. Mater. **15**, 908 (2006).
[37]N.-M. Hwang, I.-D. Jeon, and D.-Y. Kim, J. Ceramic Proc Res. **1**, 34 (2000).
[38]U. Kortshagen, J. Phys. D: Appl. Phys. **42**, 113001 (2009).
[39]J. Ma, A. Cheesman, M. N. R. Ashfold, K. G. Hay, S. Wright, N. Langford, G. Duxbury, and Y. A. Mankelevich, J. Appl. Phys. **106**, 033305 (2009).
[40]M. Frenklach, Phys. Chem. Chem. Phys. **4**, 2028 (2002).
[41]Yu. A. Mankelevich, M. A. Olevanov, and T. V. Rakhimova, Plasma Sources Sci. Technol. **17**, 015013 (2008).
[42]Yu. A. Mankelevicha, M. A. Olevanov, A. F. Pal', T. V. Rakhimova, A.N. Ryabinkin, A. O. Serov, and A. V. Filippov, Plasma Phys. Rep. **35**, 191 (2009).
[43]R. Basner, F. Sigeneger, D. Loffhagen, G. Schubert, H. Fehske, and H. Kersten, New J. Phys. **11**, 013041 (2009).

Downloaded 10 Dec 2010 to 137.222.40.127. Redistribution subject to AIP license or copyright; see http://jap.aip.org/about/rights_and_permissions